Nonuniform porosity and non-Darcian effects on conjugate mixed convection heat transfer from a plate fin in porous media

Cha'O-Kuang Chen* and Chien-Hsin Chen†
Department of Mechanical Engineering, National Cheng Kung University, Tainan, Taiwan, 70101, Republic of China

Mixed convection flow about a vertical plate fin embedded in a variable porosity medium, based on the conjugate convection–conduction theory, is analyzed. The non-Darcian effects, which include the no-slip and inertial effects, and nonuniform porosity condition are considered. Inclusion of these effects significantly alters the heat transfer from those predicted by using the Darcy flow model. For comparison, computations of heat transfer characteristics based on three velocity models, i.e., the Darcy–Brinkman–Ergun model with uniform and nonuniform porosities and the Darcy flow model, are performed. The results show that due to the near-wall porosity variation, the heat transfer rate is greatly increased. The effects of the conjugate convection–conduction parameter and the buoyancy force parameter on fin temperature distribution, the local heat transfer coefficient, local heat flux, overall heat transfer rate, and fin efficiency are illustrated.

Keywords: conjugate mixed convection; porous media

Introduction

Convective heat transfer in porous media has been studied by scientists and engineers in various disciplines. These include geophysics, hydrology, geothermal operations, heat exchange systems, packed-bed catalytic reactors, insulation engineering, and many others. Cheng[1,2] has reviewed some excellent work resulting from those investigations. Most of the existing analytical studies deal primarily with mathematical simplification based on Darcy's law, which cannot account for the effects of a solid boundary, inertial forces, and variable porosity on fluid flow and heat transfer through porous media. Boundary effects are expected to become more noticeable when heat transfer is considered in the near-wall region. Inertial effects also become important when fluid velocity is high. Non-Darcian effects, i.e., the boundary and inertial effects on heat transfer for constant-porosity media were analyzed by Vafai and Tien[3] for forced convection, and by Ranganathan and Viskanta[4] for mixed convection. Both the boundary and the inertial effects decrease fluid velocity in the thermal boundary layer and reduce heat transfer rates.

In some applications, such as fixed-bed catalytic reactors, packed-bed heat exchangers, drying, and chemical reaction engineering, the constant-porosity assumption is no longer valid. Due to the variation in packing near the solid surface, the porosity near the wall is larger than that in the main stream.[5] This leads to the occurrence of a maximum velocity in a region very close to the wall, called flow channeling.[6,7] The variable-porosity effects on convective flow and heat transfer were examined by Vafai[8] for forced convection and by Hong *et al.*[9] for natural convection. They showed that the flow-channeling effect significantly increases the heat transfer rate.

Conventional studies of heat transfer in porous media are based on assumed temperature distributions along the impermeable surface. In many of the applications cited, taking into consideration the interaction between the solid boundary and its adjacent boundary-layer flow would more closely approximate the physical situation. Thus, in the analysis of heat transfer from a long fin, it is more realistic to leave the heat transfer coefficient unspecified and treat it as part of the solution. Conjugate heat transfer problems induced by various convection mechanisms have been investigated extensively.[10–13] In recent papers by Liu *et al.*,[14,15] the analysis has been extended to include conjugate mixed convection–conduction heat transfer in porous media using Darcy's law. More recently, boundary and inertial effects on conjugate mixed convection heat transfer in a constant high-porosity medium were examined by Gill and Minkowycz[16] in a similar analysis.

In the present investigation, attention is given to the non-Darcian and nonhomogeneous effects on conjugate mixed convection–conduction heat transfer in a packed-sphere bed. The Darcy–Brinkman–Ergun model is used as the momentum equation, with the porosity variation of the packed bed approximated by an exponential function. The boundary-layer equations are coupled with the one-dimensional (1-D) heat conduction equation in the fin through interfacial conditions. Numerical solutions of the governing differential equations are generated by an efficient finite difference method. Finally, the qualitative effects of the controlling parameters on heat transfer are demonstrated graphically.

Analysis

Consider the problem of the boundary-layer flow along a vertical plate fin of length L and thickness 2δ, which is embedded

* Professor
† Graduate student

Address reprint requests to Professor Chen at the Department of Mechanical Engineering, National Cheng Kung University, Tainan, Taiwan, 70101, Republic of China.

Received 2 November 1988; accepted 12 June 1989

© 1990 Butterworth Publishers

vertically downward in a fluid-saturated porous medium at an ambient temperature of T_∞, as shown in Figure 1. The fin base temperature is maintained at a constant temperature T_b, which is higher than T_∞. The coordinate system—with the origin at the tip of the fin—is oriented so that the gravitational force acts in the negative x-direction and the y-axis is perpendicular to the fin surface. At free stream, a uniform flow with velocity u_∞ is flowing in the positive x-direction. Thus the buoyancy force is acting in the same direction as the external flow. Under the assumptions that the fluid and the porous medium are in local thermal equilibrium—and that the boundary-layer

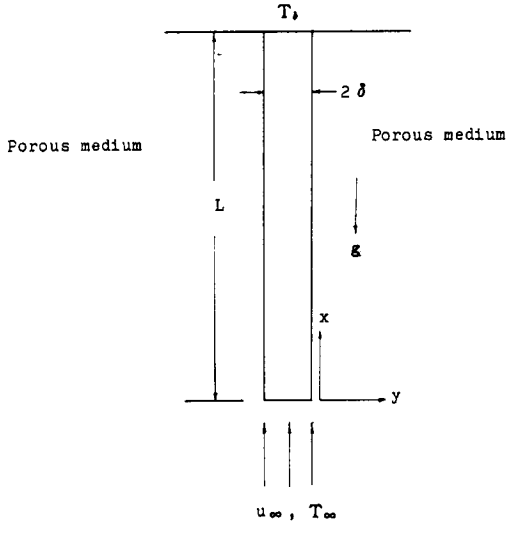

Figure 1 Schematic diagram of the physical problem

and Boussinesq approximations are applicable—the governing equations for flow in the porous medium, with the momentum equation based on the Darcy–Brinkman–Ergun model, are[3]

$$\frac{\mu}{K(y)}u+\rho C(y)u^2=-\frac{\partial p}{\partial x}+\rho g\beta(T-T_\infty)+\frac{\mu}{\phi}\frac{\partial^2 u}{\partial y^2} \tag{1}$$

$$u\frac{\partial T}{\partial x}+v\frac{\partial T}{\partial y}=\alpha\frac{\partial^2 T}{\partial y^2} \tag{2}$$

where u and v are the velocity components in the x- and y-directions; T, p, and g are the temperature, pressure, and gravitational constant; ρ, μ, and β are the density, viscosity, and thermal expansion coefficient of the fluid; α is the effective thermal diffusivity of the saturated porous medium; $K(y)$ and $C(y)$ are the permeability and inertial coefficient of the porous medium; and ϕ is the porosity of the packed bed. The functional dependence of the porosity on the distance y from the wall can be found from the experimental work by Benenati and Brosilow.[5] Although the porosity variation oscillates, a simple exponential function is usually assumed to account for the effect of non-homogeneity, as used by several investigators[8,9,17]:

$$\phi=\phi_\infty\left[1+b\exp\left(\frac{-cy}{d}\right)\right] \tag{3}$$

This representation neglects the small oscillations of porosity, which are considered to be secondary. The emphasis here is on the decay of porosity from the solid wall, which has the primary effect. Here $\phi_\infty=0.4$ is the free-stream porosity, y is the distance from the wall, d is the sphere diameter, and b and c are experimental parameters, that depend on the packing of the spheres near the solid wall. We chose the value of b so that the porosity at the wall is ϕ_w and the value of c to approximate porosity decay. The Darcian and inertial terms in the momentum

Notation

b Porosity-variation parameter (Equation 3)
C Inertial coefficient (Equation 1)
c Porosity-variation parameter (Equation 3)
Da Darcy number, K_∞/L^2
d Particle diameter
f Dimensionless stream function
g Gravitational constant
h Local heat transfer coefficient
$\hat{h}$ Dimensionless local heat transfer coefficient, $hL/(k\sqrt{\mathrm{Re}})$
$\bar{h}$ Average heat transfer coefficient (Equation 30)
K Permeability
k Effective thermal conductivity of the porous medium
k_f Fin thermal conductivity
L Fin length
N_c Convection–conduction parameter, $kL\sqrt{\mathrm{Re}}/(k_f\delta)$
Pe Peclet number, $u_\infty L/\alpha$
Pr Prandtl number, v/α
p Pressure
Q Overall heat transfer rate (Equation 34)
$\tilde{Q}$ Dimensionless overall heat transfer rate, $Q/(k(T_b-T_\infty)\sqrt{\mathrm{Re}})$
q Local heat flux
$\hat{q}$ Dimensionless local heat flux, $qL/(k(T_b-T_\infty)\sqrt{\mathrm{Re}})$
Re Reynolds number, $u_\infty L/v$
T Temperature
u Velocity in x-direction
v Velocity in y-direction
x Streamwise coordinate
y Cross-stream coordinate

Greek letters
α Effective thermal diffusivity
β Coefficient of thermal expansion
δ Plate fin half thickness
η Pseudosimilarity variable (Equation 14)
η_{eff} Fin efficiency (Equation 38)
θ Dimensionless temperature
Λ Inertial parameter, $C_\infty K_\infty u_\infty/v$
μ Dynamic viscosity of fluid
v Kinematic viscosity of fluid
ξ Dimensionless streamwise coordinate
ρ Density of fluid
ϕ Porosity
ψ Stream function
Ω Buoyancy force parameter, $g\beta K_\infty(T_b-T_\infty)/(vu_\infty)$

Subscripts
b Condition at the fin base
f Quantities associated with the fin
w Condition at the wall
∞ At a distance from the wall

Superscripts
$'$ Differentiation with respect to η

equation contain the empirical coefficients K and C, which are determined from the well-known correlations developed by Ergun[18] for flow in a packed bed:

$$K=\frac{d^2\phi^3}{150(1-\phi)^2} \tag{4}$$

$$C=\frac{1.75(1-\phi)}{d\phi^3} \tag{5}$$

The boundary conditions for Equations 1 and 2 are

$$u=v=0; \quad T=T_w(x) \quad \text{at} \quad y=0 \tag{6}$$

$$u=u_\infty; \quad T=T_\infty \quad \text{as} \quad y\to\infty \tag{7}$$

If the thickness of the fin is relatively small compared to its length, heat conduction within the fin can be considered to be 1-D. Accordingly, the governing equation for temperature distribution along the fin is

$$k_f\delta\frac{d^2T_f}{dx^2}=h(x)(T_f-T_\infty) \tag{8}$$

where T_f is the temperature of the fin, k_f is the thermal conductivity of the fin, $h(x)$ is the local heat transfer coefficient, which is unknown at present and will be obtained as part of the solution. The boundary conditions for the fin are

$$\frac{dT_f}{dx}=0 \quad \text{at} \quad x=0 \tag{9}$$

$$T_f(x)=T_b \quad \text{at} \quad x=L \tag{10}$$

where the heat loss from the tip of the fin is assumed to be negligible.

The boundary layer equations are coupled with the fin conservation equation through the following interfacial conditions:

$$T(x,y)=T_f(x) \quad \text{at} \quad y=0 \tag{11}$$

$$-k\frac{\partial T}{\partial y}(x,y)=h(x)(T_f(x)-T_\infty) \quad \text{at} \quad y=0 \tag{12}$$

These two conditions state the physical requirements that the temperature and heat fluxes of the fin and the porous medium must be continuous across the fin–fluid interface.

To facilitate the analysis, the following transformations are introduced to nondimensionalize the preceding equations

$$\xi=\frac{x}{L} \tag{13}$$

$$\eta=y\sqrt{\frac{u_\infty}{\alpha x}} \tag{14}$$

$$\psi=\sqrt{\alpha u_\infty x}\,f(\xi,\eta) \tag{15}$$

$$\theta=\frac{T-T_\infty}{T_b-T_\infty} \tag{16}$$

$$\theta_f=\frac{T_f-T_\infty}{T_b-T_\infty} \tag{17}$$

where the stream function ψ is defined as

$$u=\frac{\partial\psi}{\partial y} \quad \text{and} \quad v=-\frac{\partial\psi}{\partial x} \tag{18a,b}$$

When the transformations given by Equations 13–16 are applied to Equations 1 and 2,

$$\frac{\mathrm{Pe\,Da}}{\phi\xi}f'''-\left(\frac{C}{C_\infty}\right)\Lambda(f')^2-\left(\frac{K_\infty}{K}\right)f'+\Omega\theta+1+\Lambda=0 \tag{19}$$

$$\theta''+\tfrac{1}{2}f\theta'=\xi\left(f'\frac{\partial\theta}{\partial\xi}-\theta'\frac{\partial f}{\partial\xi}\right) \tag{20}$$

where

$$\mathrm{Da}=\frac{K_\infty}{L^2}$$

$$\mathrm{Pe}=\frac{u_\infty L}{\alpha}$$

$$\Lambda=\frac{C_\infty K_\infty u_\infty}{\nu}$$

and

$$\Omega=\frac{g\beta K_\infty(T_b-T_\infty)}{\nu u_\infty}$$

is the buoyancy-force parameter, which is a measure of the relative importance of free convection to forced convection. After the transformation, Equations 6 and 7 become

$$f'=0; \quad \xi\frac{\partial f}{\partial\xi}+\tfrac{1}{2}f=0; \quad \theta=\theta_w \quad \text{at} \quad \eta=0 \tag{21a–c}$$

$$f'=1; \quad \theta=0 \quad \text{as} \quad \eta\to\infty \tag{22a,b}$$

where the primes indicate differentiation with respect to η. Equations 8–10 can be expressed in the following dimensionless form:

$$\frac{d^2\theta_f}{d\xi^2}=N_c\hat{h}(\xi)\theta_f \tag{23}$$

$$\xi=0: \frac{d\theta_f}{d\xi}=0 \tag{24}$$

$$\xi=1: \theta_f=1 \tag{25}$$

where $N_c=kL\sqrt{\mathrm{Re}}/k_f\delta$ and $\hat{h}(\xi)=hL/k\sqrt{\mathrm{Re}}$ are the conjugate convection–conduction parameter and the dimensionless local heat transfer coefficient, respectively.

The interfacial conditions in terms of the new variables are

$$\theta=\theta_f \quad \text{at} \quad \eta=0 \tag{26}$$

$$-\theta'=\frac{\hat{h}(\xi)\sqrt{\xi}\,\theta_f}{\sqrt{\mathrm{Pr}}} \quad \text{at} \quad \eta=0 \tag{27}$$

where $\mathrm{Pr}=\nu/\alpha$ is the Prandtl number. Equations 19–27 constitute the governing equations and boundary conditions for the present problem. This complete set of equations must be solved simultaneously because of the coupling of the system. Numerical solutions for the entire set of equations, Equations 19–27, was obtained by using a modified version of the implicit finite-difference technique.[19] The details of the computational procedure are similar to those described in Ref. 10 and will not be repeated here.

Results and discussion

The numerical results—with a focus on the non-Darcian, nonuniform porosity, buoyancy, and nonisothermal effects—are presented for a packed-sphere bed with particle size $d=5$ mm. The free-stream permeability and inertial coefficient can be calculated from Equations 4 and 5. The values of empirical constants b and c in Equation 3 are 1 and 6,[20] respectively. In obtaining the computational results, we also used the following values of input parameters: $\mathrm{Pr}=4.35$, $\mathrm{Re}=12{,}490$ for water at $\nu=0.8007\times10^{-6}$ m^2/s, $L=0.5$ m, and

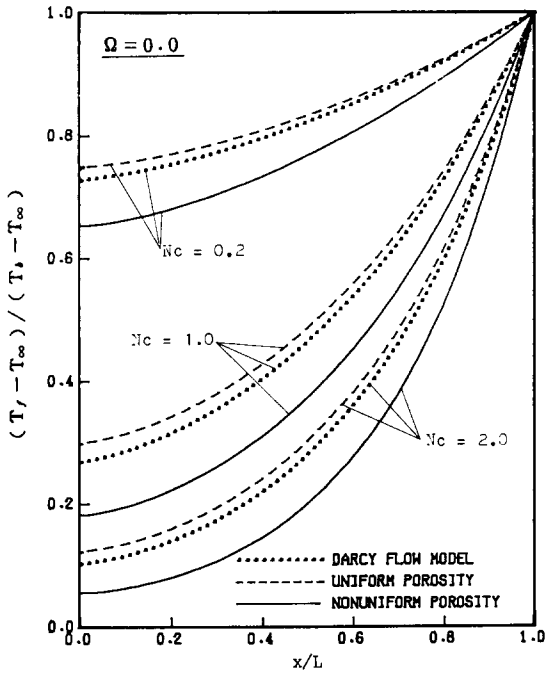

Figure 2 Fin temperature distributions for $\Omega=0$

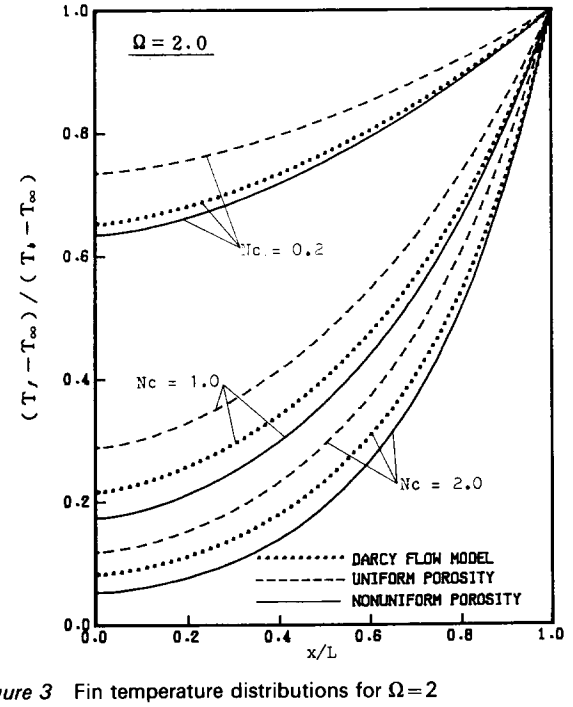

Figure 3 Fin temperature distributions for $\Omega=2$

$u_\infty=0.02$ m/s. The convection–conduction number N_c and mixed convection parameter Ω are considered in the range of 0–2.0. The figure legends identify the three different flow models considered: *uniform porosity* and *nonuniform porosity*, which refer to the Darcy–Brinkman–Ergun model with uniform and nonuniform porosities, respectively, and the *Darcy flow model*.

Results for the fin temperature distributions are presented for some selected values of N_c in Figure 2 for pure forced convection ($\Omega=0$) and in Figure 3 for mixed convection ($\Omega=2.0$). Comparing these values with the results based on the Darcy flow model shows that in all cases the non-Darcian effects decrease fin temperature variations, and nonuniform porosity effects increase fin temperature variations significantly. The reason is that nonhomogeneity enhances convective heat transfer, resulting in lower temperatures. Fin temperature distributions also depend on the parameters N_c and Ω. All of the fin temperature distributions increase monotonically from the tip of the fin to the base. Figures 2 and 3 show that larger values of N_c predict larger base-to-tip temperature variations. The basic cause of this behavior is that larger values of N_c correspond to lower fin conductances and higher convective cooling, which promote greater fin temperature nonuniformities. Higher fin temperature variations are also seen in mixed convection flows. This is evident from the fact that the buoyancy force assists the flow and thus enhances heat transfer rates.

In terms of its usual definition, the local heat transfer coefficient of the fin can be expressed as

$$h(x)=-\frac{k\left.\dfrac{\partial T}{\partial y}\right|_{y=0}}{(T_f-T_\infty)} \tag{28}$$

or in dimensionless form as

$$\hat{h}(\xi)=\frac{hL}{(k\sqrt{\mathrm{Re}})}=-\frac{\sqrt{\mathrm{Pr}}\,\theta'(\xi,0)}{(\sqrt{\xi}\,\theta_f)} \tag{29}$$

Figures 4 and 5 show the representative distributions of this quantity along the fin surface for pure forced convection and mixed convection based on various flow models. As these figures show, the non-Darcian effects reduce the local heat transfer coefficients in uniform-porosity media. The coefficients are increased because of the nonhomogeneity in porosity. Similar results are reported in Ref. 9.

For a pure forced convection flow at low N_c ($N_c=0.2$), the local heat transfer coefficient decreases along the increasing streamwise direction, with relatively fast changes near the fin tip and more gradual changes downstream. For the larger value of N_c ($N_c=2.0$), the h values begin with a sharp drop near the fin tip and then tend to level off, taking on more constant values.

Consider now mixed convection flows, as shown in Figure 5.

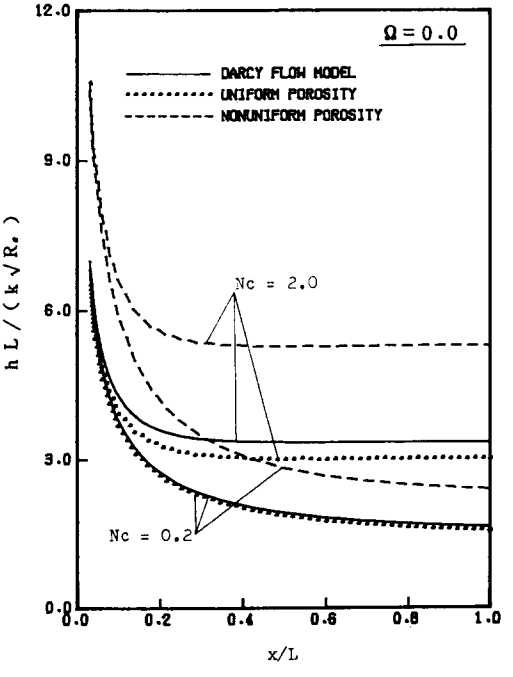

Figure 4 Local heat transfer coefficients for $\Omega=0$

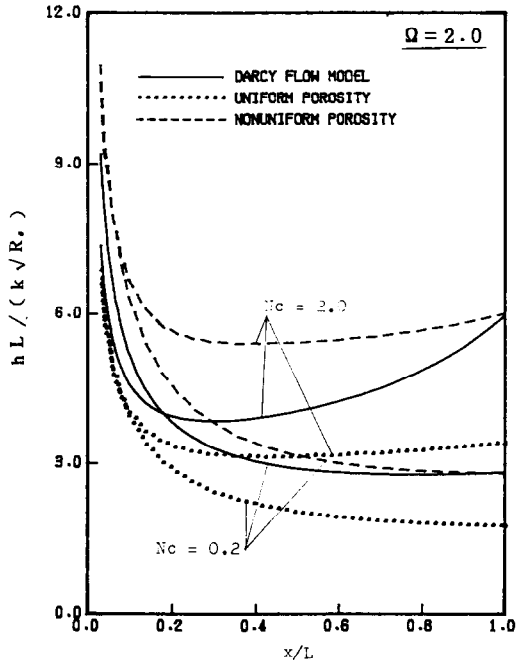

Figure 5 Local heat transfer coefficients for $\Omega=2$

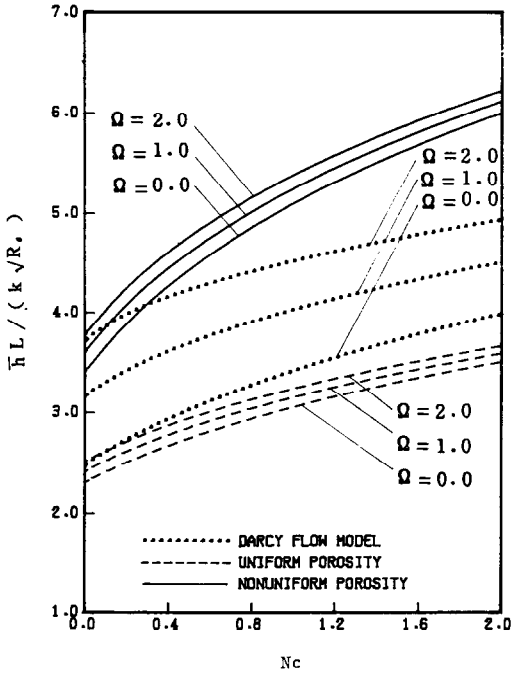

Figure 6 Average heat transfer coefficients

At higher values of N_c, the coefficients decrease rapidly at first, attain a minimum, and then increase steadily with ξ. This behavior results from an enhanced buoyancy force along the streamwise direction, which further accelerates the flow. Figure 5 also reveals that the local heat transfer coefficients decrease monotonically in the direction of fluid flow at the smaller value of N_c.

The average heat transfer coefficient can be obtained from

$$\bar{h}=\frac{1}{L}\int_0^L h(x)\,dx \tag{30}$$

which can be cast in dimensionless form as

$$\frac{\bar{h}L}{k\sqrt{\mathrm{Re}}}=\int_0^1 \hat{h}(\xi)\,d\xi \tag{31}$$

The numerical results of this quantity are given in Figure 6. It is obvious that as a consequence of near-wall porosity variation, higher values of average heat transfer coefficients prevail in flows through variable-porosity media. Also, the average heat transfer coefficients increase with increasing N_c or Ω.

The local heat flux along the fin surface can be expressed as

$$q(x)=-k\left.\frac{\partial T}{\partial y}\right|_{y=0} \tag{32}$$

or

$$\hat{q}(\xi)=\frac{qL}{k(T_b-T_\infty)\sqrt{\mathrm{Re}}}=-\theta'(\xi,0)\sqrt{\frac{\mathrm{Pr}}{\xi}} \tag{33}$$

Figures 7 and 8 present distributions of the dimensionless local heat flux at the fin surface. For given values of the convection–conduction parameter and the buoyancy force parameter, it is clear from the figures that the non-Darcian effects decrease the local heat flux and the effect of nonuniform porosity is to increase this quantity. Comparing Figures 7 and 8 reveals that, because of buoyancy, the local heat fluxes for mixed convection are higher than those for pure forced convection. The results also show that as N_c increases, most of the heat flux is convected to the fluid near the fin base. This effect is attributed to the fact that a higher value of N_c, representing a lower thermal conductivity of the fin, yields a higher temperature near the base.

The overall rate of heat transfer can be computed either from the integration of local convective flux at the fin surface or from the heat conduction from the base into the fin at $\xi=1.0$. In dimensional terms, we have

$$Q=2\int_0^L q(x)\,dx \tag{34}$$

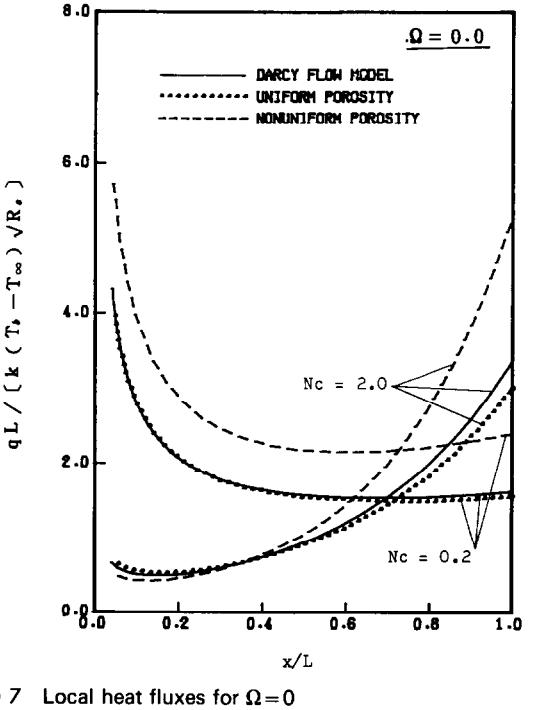

Figure 7 Local heat fluxes for $\Omega=0$

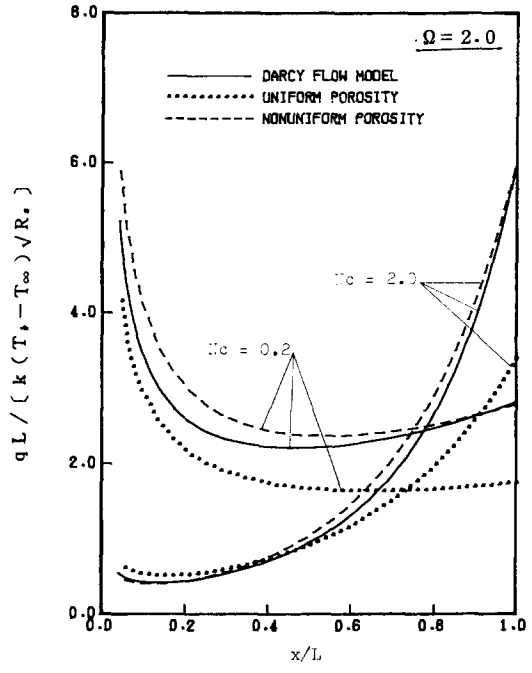

Figure 8 Local heat fluxes for $\Omega = 2$

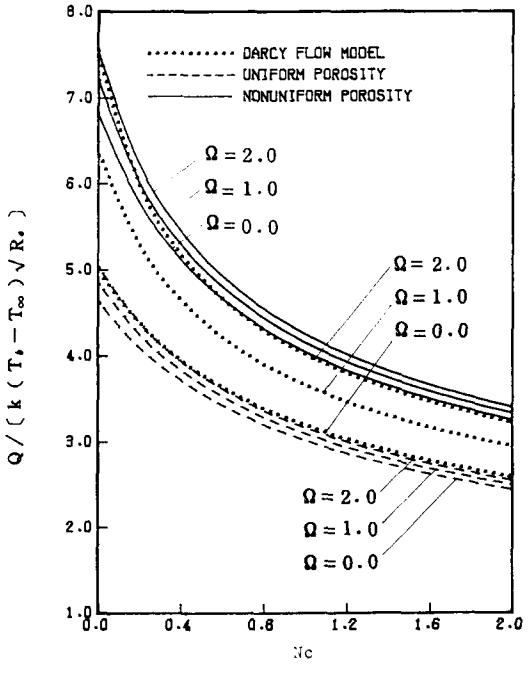

Figure 9 Overall heat transfer rates

$$Q = 2k_f \delta \left.\frac{dT_f}{dx}\right|_{x=L} \tag{35}$$

When dimensionless variables are introduced,

$$\hat{Q} = \frac{Q}{k(T_b - T_\infty)\sqrt{\mathrm{Re}}} = 2\int_0^1 \hat{q}(\xi)\, d\xi \tag{36}$$

or

$$\hat{Q} = \frac{Q}{k(T_b - T_\infty)\sqrt{\mathrm{Re}}} = \frac{2}{N_c}\left.\frac{d\theta_f}{d\xi}\right|_{\xi=1} \tag{37}$$

Numerical values of Q obtained from both approaches are found to be in excellent agreement. Results of the dimensionless Q are plotted in Figure 9 as a function of N_c. This figure shows that the overall heat transfer rates decrease because of the non-Darcian effects and increase because of porosity variation. These results agree with the previous results for local heat fluxes. They also show that the overall heat transfer rate decreases with an increasing N_c and a decreasing Ω. A higher value of N_c represents a more nonisothermal fin, and therefore results in a smaller value of the overall heat transfer rate. The effect of the buoyancy force is to enhance the heat transfer rate, as expected.

The fin efficiency compares the heat transfer for a real fin with that for an isothermal fin. With this definition, we have

$$\eta_{\mathrm{eff}} = \frac{Q}{Q_{\mathrm{iso}}} \tag{38}$$

where Q_{iso} denotes the overall heat transfer rate resulting from an isothermal fin. The results of η_{eff} *versus* N_c are presented in Figure 10 for representative values of Ω. Fin efficiency is also regarded as a measure of the departure of the fin temperature distribution from a uniform T_b. Thus the downsloping curves indicate that larger values of N_c give rise to greater fin temperature nonuniformities and less efficiency. Note also that the heat transfer rate from the corresponding isothermal fin is not the same for flows based on different models. Therefore a greater efficiency does not imply a higher heat transfer rate for different flows.

Conclusions

An analysis was performed to obtain the solution to the problem of conjugate mixed convection from a vertical plate fin embedded in a porous medium, taking into consideration non-Darcian and nonuniform porosity effects. Three flow models were used to show the importance of porosity on heat transfer in variable porosity media. We found that the effect of porosity variation is to increase fin temperature nonuniformities, heat transfer coefficients, and heat transfer rates; non-Darcian terms result in reverse effects. The influence of other governing parameters

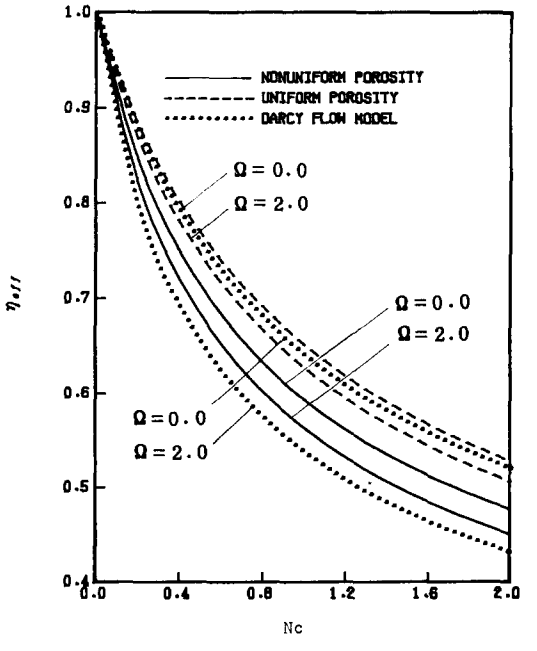

Figure 10 Fin efficiencies

on the predicted heat transfer characteristics was discussed in detail. Nonmonotonical local heat transfer distributions are observed at a high conjugate convection–conduction parameter. This behavior is similar to the case of classic fluids.

References

1 Cheng, P. Heat transfer in geothermal systems. *Adv. Heat Transf.* 1978, **14**, 1–105

2 Cheng, P. Natural convection in porous medium: External flows. Paper presented to the NATO Advanced Study Institute on Natural Convection: Fundamentals and Applications, Izmir, Turkey, July 16–27, 1984

3 Vafai, K. and Tien, C. L. Boundary and inertia effects of flow and heat transfer in porous media. *Int. J. Heat and Mass Transf.* 1981, **24**, 195–203

4 Ranganathan, R. and Viskanta, R. Mixed convection boundary layer flow along a vertical porous medium. *Numer. Heat Transf.* 1984, **7**, 305–317

5 Benenati, R. F. and Brosilow, C. B. Void fraction distribution in beds of spheres. *AIChE J.* 1962, **8**, 359–361

6 Schert, W. M. and Bishoff, K. B. Thermal and material transport in non-isothermal packed beds. *AIChE J.* 1969, **15**, 597–604

7 Schwartz, C. E. and Smith, J. M. Flow distribution in packed beds. *Ind. Eng. Chem.* 1953, **45**, 1209–1218

8 Vafai, K. Convective flow and heat transfer in variable-porosity media. *J. Fluid Mech.* 1984, **147**, 233–259

9 Hong, J. T., Yamada, Y., and Tien, C. L. Effects of non-Darcian and nonuniform porosity on vertical-plate natural convection in porous media. *J. Heat Transf.* 1987, **109**, 356–362

10 Sparrow, E. M. and Acharya, S. A natural convection fin with a solution-determined nonmonotonically varying heat transfer coefficient. *J. Heat Transf.* 1981, **103**, 218–225

11 Sparrow, E. M. and Chyu, M. K. Conjugate forced convection–conduction analysis of heat transfer in a plate fin. *J. Heat Transf.* 1982, **104**, 204–206

12 Huang, M. J., Chen, C. K., and Cleaver, J. W. Vertical circular pin with conjugate natural convection–conduction flow. *J. Heat Transf.* 1985, **107**, 242–245

13 Huang, M. J. and Chen, C. K. Conjugate mixed convection and conduction heat transfer along a vertical circular pin. *Int. J. Heat and Mass Transf.* 1985, **28**, 523–529

14 Liu, J. Y., Minkowycz, W. J., and Cheng, P. Conjugate mixed convection heat transfer analysis of a plate fin embedded in a porous medium. *Numer. Heat Transf.* 1986, **9**, 575–590

15 Liu, J. Y., Minkowycz, W. J., and Cheng, P. Conjugate mixed convection–conduction heat transfer along a cylindrical fin in a porous medium. *Int. J. Heat and Mass Transf.* 1986, **29**, 769–775

16 Gill, U. S. and Minkowycz, W. J. Boundary and inertia effects on conjugate mixed convection heat transfer from a vertical plate fin in a high-porosity porous medium. *Int. J. Heat and Mass Transf.* 1988, **31**, 419–427

17 Vortmeyer, D. and Schuster, J. Evaluation of steady flow profiles in rectangular and circular packed beds. *Chem. Eng. Sci.* 1983, **38**, 1691–1699

18 Ergun, S. Fluid flow through packed columns. *Chem. Eng. Prog.* 1952, **48**, 89–94

19 Cebeci, T. and Bradshaw, P. *Momentum Transfer in Boundary Layers*. Hemisphere, Washington, D.C., 1977

20 Cheng, P. Private communication, Department of Mechanical Engineering, University of Hawaii at Manoa, USA